

Identification of the biogenic compounds responsible for size-dependent nanoparticle growth

Paul M. Winkler,^{1,2} John Ortega,¹ Thomas Karl,¹ Luca Cappellin,³ Hans R. Friedli,¹ Kelley Barsanti,⁴ Peter H. McMurry,⁵ and James N. Smith^{1,6}

Received 30 July 2012; revised 28 September 2012; accepted 3 October 2012; published 30 October 2012.

[1] The probability that freshly nucleated nanoparticles can survive to become cloud condensation nuclei is highly sensitive to particle growth rates. Much of the growth of newly formed ambient nanoparticles can be attributed to oxidized organic vapors originating from biogenic precursor gases. In this study we investigated the chemical composition of size-selected biogenic nanoparticles in the size range from 10 to 40 nm. Particles were formed in a flow tube reactor by ozonolysis of α -pinene and analyzed with a Thermal Desorption Chemical Ionization Mass Spectrometer. While we found similar composition in 10 and 20 nm particles, the relative amounts of individual species varied significantly when compared to 40 nm particles. Smaller particles (10 and 20 nm) were characterized by enhancements in carboxylic acids and larger particles (40 nm) showed higher concentrations of carbonyl-containing compounds and low molecular weight organic acids. This composition change from smaller to larger size particles reflects a vapor pressure increase of the condensing vapors by 1–2 orders of magnitude indicating that the Kelvin effect plays a decisive role in the growth of biogenic nanoparticles. **Citation:** Winkler, P. M., J. Ortega, T. Karl, L. Cappellin, H. R. Friedli, K. Barsanti, P. H. McMurry, and J. N. Smith (2012), Identification of the biogenic compounds responsible for size-dependent nanoparticle growth, *Geophys. Res. Lett.*, 39, L20815, doi:10.1029/2012GL053253.

1. Introduction

[2] The formation of nanoparticles by gas-to-particle conversion is frequently observed in the atmosphere and constitutes a major source of ambient aerosol in the submicron size range [Kulmala *et al.*, 2004]. Potential health risks associated with the inhalation of nanoparticles as well as their expected impact on global climate through the formation of cloud condensation nuclei have led to an increased demand for understanding the underlying formation mechanisms.

The typical pathway currently considered is nucleation followed by growth due to condensation [Kulmala, 2003]. Recent chamber studies have shown that ambient particle formation rates can be described reasonably well by multi-component nucleation involving sulfuric acid and ammonia or amines [Kirkby *et al.*, 2011], but ambient levels of sulfuric acid are rarely sufficient to describe the high growth rates observed in the atmosphere [Weber *et al.*, 1997; Boy *et al.*, 2005; Stolzenburg *et al.*, 2005]. Instead, the major constituents of freshly formed nanoparticles were identified to be of organic origin suggesting that organic vapors account for the rapid growth of nanoparticles [Smith *et al.*, 2008; Wehner *et al.*, 2005].

[3] The importance of correctly quantifying growth rates can be seen from equation (1) [McMurry and Friedlander, 1979; Weber *et al.*, 1997],

$$J(D_p) = J_1 \cdot \exp\left(-\frac{kA_{Fuchs}}{dD_p/dt}\Psi\right), \quad (1)$$

where the formation rate $J(D_p)$ of particles with diameter D_p is related to the formation rate J_1 of 1 nm particles via an exponential function showing the diameter growth rate dD_p/dt in the denominator. An expression equivalent to equation (1) was described by Kerminen and Kulmala [2002]. A_{Fuchs} is the “Fuchs surface area” [McMurry, 1983], representing coagulation efficiency, and k and Ψ are kinetic factors determined from theory. Accordingly, only if dD_p/dt is sufficiently large compared to scavenging by coagulation will a significant number of ~ 1 nm particles survive and grow to larger sizes. A “successful” particle formation event is thus governed by a high growth rate or a low coagulation sink.

[4] In order to better understand mechanisms responsible for nanoparticle growth we employ a Thermal Desorption Chemical Ionization Mass Spectrometer (TDCIMS) [Voisin *et al.*, 2003; Smith *et al.*, 2004] providing chemical speciation of size-selected particles typically in the size range between 10 and 40 nm. In this study our focus is on laboratory generated secondary organic aerosol (SOA) formed by the ozonolysis of α -pinene. Although this system has been widely studied due to its atmospheric relevance, little information is available on the initial steps of particle formation. Here we present new insights into properties of biogenic nanoparticles that have just outgrown the cluster regime.

2. Experiment

[5] A schematic of the experimental setup as well as typical operating conditions of the flow tube reactor used for SOA formation are shown in Figure S1 in Text S1 of the

¹Atmospheric Chemistry Division, National Center for Atmospheric Research, Boulder, Colorado, USA.

²Now at Faculty of Physics, University of Vienna, Vienna, Austria.

³Food Quality and Nutrition Area, IASMA Research and Innovation Centre, Fondazione Edmund Mach, San Michele, Italy.

⁴Department of Civil and Environmental Engineering, Portland State University, Portland, Oregon, USA.

⁵Department of Mechanical Engineering, University of Minnesota, Twin Cities, Minneapolis, Minnesota, USA.

⁶Department of Applied Physics, University of Eastern Finland, Kuopio, Finland.

Corresponding author: P. M. Winkler, Faculty of Physics, University of Vienna, Vienna AT-1090, Austria. (pwinkler@ucar.edu)

©2012. American Geophysical Union. All Rights Reserved.
0094-8276/12/2012GL053253

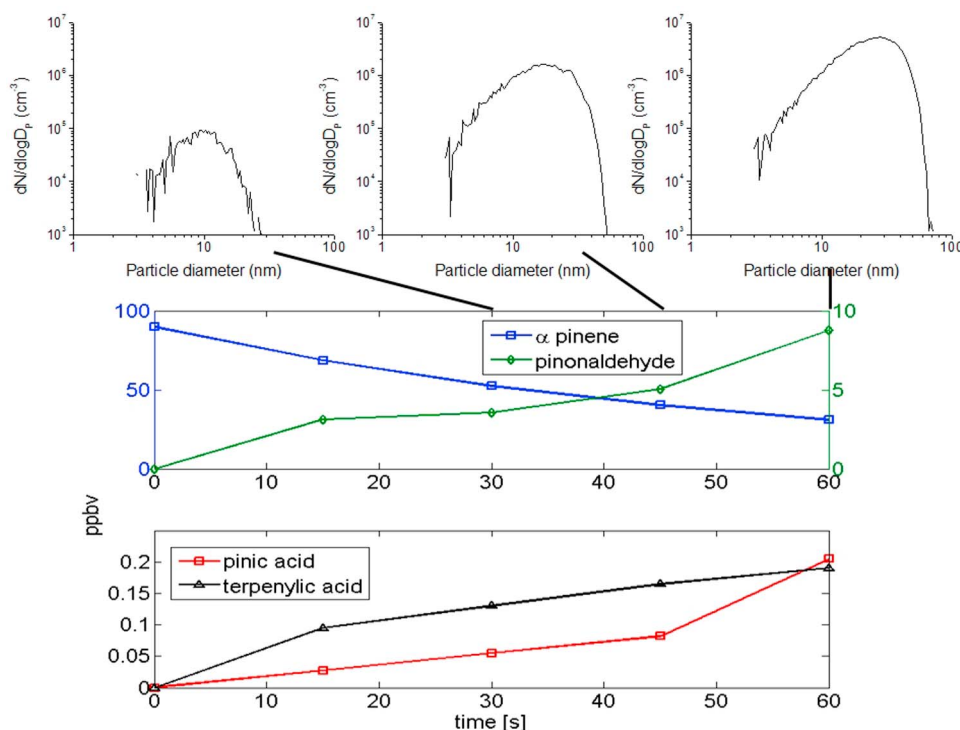


Figure 1. Selected gas-phase species concentrations at different residence times as measured with the PTR-TOF-MS. Blue shows the decrease of α -pinene (+137.132) over time whereas green shows the increase of pinonaldehyde (+169.125). Black (terpenylic acid, +173.078) and red (pinic acid, +187.088) show the increase of two dominant dicarboxylic acids with time. Note the scale change in the concentration. On top are shown the size distribution data measured with the SMPS at residence times 30, 45 and 60 s. No particles were measured at 15 s.

auxiliary material.¹ The major advantage of conducting these experiments in a flow tube as opposed to an environmental chamber is that by choosing a proper residence time, a stable aerosol with a certain size distribution and sufficiently high number concentration can be maintained for hours or even days. This allows much higher sample collection compared to chamber studies, which is essential for the characterization of 10 nm particle composition.

[6] A comprehensive suite of instruments was used to characterize gas-phase composition, size distribution evolution and particle chemical composition. Ozone concentration was measured using a photometric ozone analyzer [Thermo Electron, model 49]. Gas-phase volatile organic compounds (VOCs) were monitored by a Proton Transfer Reaction Time-of-Flight Mass Spectrometer (PTR-TOF-MS) [Jordan *et al.*, 2009]. This instrument has sufficiently high mass resolution as to allow the quantitative determination of VOCs up to m/z 500. Instrumental setup and calibration procedures for the PTR-TOF-MS are described in the auxiliary material. Particle size distributions were monitored using a scanning mobility particle sizer (SMPS) comprising of a nanometer differential mobility analyzer (nano DMA, TSI Inc., model 3085) and an ultrafine condensation particle counter (UCPC, TSI Inc., model 3025).

[7] The chemical composition of size-selected particles was measured using the TDCIMS. This system uses a low resolution electrostatic classification technique [McMurtry

et al., 2009] to collect samples of aerosol nanoparticles on a metal filament and then resistively heats the filament and analyzes the desorbed gas using chemical ionization mass spectrometry. In separate but complementary experiments, a quadrupole and a high-resolution time-of-flight (HTOF) mass spectrometer were used. Quantitative analysis of the mass spectra was performed on the quadrupole system, whereas the HTOF was used to identify the exact chemical formulae of the peaks. Since the TDCIMS relies on thermal desorption of sampled aerosol in its analysis, any oligomers that may be formed in particles most likely decompose into their respective monomers [Hall and Johnston, 2012]. In reporting both HTOF-TDCIMS and PTR-TOF-MS measurements below, molecular compounds are assigned based on exact molecular composition with the caveat that neither instrument is capable of distinguishing structural isomers.

3. Results

3.1. Gas-Phase Measurements

[8] The gas-phase evolution due to the ozonolysis was measured at four different residence times (15, 30, 45 and 60 s). Figure 1 depicts the time evolution of the precursor vapor and three reaction product ions for the first 60 s, which are characterized by an exponential decrease of α -pinene and reaction intermediates that increase over time. The measured decrease of α -pinene followed a predicted evolution using the Leeds Master Chemical Mechanism (MCM) [Saunders *et al.*, 2003], where the OH concentration was calculated to be on the order of 10^8 molecules cm^{-3} (see auxiliary

¹Auxiliary materials are available in the HTML. doi:10.1029/2012GL053253.

material, Figure S2). Based on this, the combined lifetime of α -pinene due to OH and O_3 oxidation is then calculated as 68 s, close to what has been estimated from Figure 1. The MCM predicts RO₂ levels for these experiments (ref. Figure S2) that are higher than those found in the atmosphere; if accurate, this can affect the identity and yields of reaction products [Jenkin, 2004]. For this simple system the PTR-TOF-MS detected more than 450 ions due to oxidation chemistry. While a complete interpretation of the mass spectrum is beyond the scope of this paper we focus on key species that are known to be produced during the oxidation of α -pinene. Figure 1 shows that during the course of the experiment pinonaldehyde concentrations increased to about 9 ppbv while the dominant organic acids, pinic acid and terpenylic and/or cis-norpinonic acid, increased to about 0.2 ppbv under NO_x-free conditions. These organic acids have been identified as major constituents in organic aerosol [Claeys *et al.*, 2009] and, as shown below, also correspond to ion peaks at m/z 171 and 185 observed in the TDCIMS negative ion mass spectra.

3.2. Particle-Phase Measurements

[9] Also shown in Figure 1 is the evolution of the particle size distribution as a function of residence time. While few particles are produced during the first 30 s, a steep increase in particle number and size is observed at 45 s reaction time. The latter residence time was used for particle analysis with the TDCIMS as the corresponding size distribution exhibits all sizes of interest at sufficient number concentration and coagulation effects can still be regarded negligible. After 60 s the peak of the size distribution appears at about 30 nm corresponding to a diameter growth rate of $\sim 30 \text{ nm min}^{-1}$. Furthermore it is notable that particles smaller than 10 nm appear at much lower concentrations at all residence times preventing analysis of particle sizes below 10 nm.

3.2.1. Aerosol Volatility and the Effects of Sampling Time

[10] Particle composition data have been obtained for particle mobility diameters of 10, 20 and 40 nm. For sufficient signal-to-noise ratios sampled particulate masses in the order of 10 ng are desired. To compensate for the substantially smaller masses in the smallest particles, the collection time must be increased relative to that of larger particles. A quantitative comparison between samples of different particle sizes collected over different periods of time is only possible if the composition of the collected sample does not change during collection, e.g., by evaporation of semi-volatile constituents. We therefore present results of measured composition of aerosol formed under identical flow tube conditions, but sampled for different lengths of time.

[11] As a consequence of the size distribution where 20 nm particles are close to the maximum of the distribution and larger 40 nm particles are in the tail at much lower concentration (Figure 1), both 20 and 40 nm diameter particles were collected for 30 minutes yielding mass loadings of about 12 ng at each size. The much lower concentration and mass of the 10 nm particles necessitated collecting for 3 and 6 hours to obtain mass loadings of ~ 3 and 6 ng, respectively.

[12] Under otherwise identical experimental conditions, except a doubling of collection time, one would expect a doubling of the ion abundances in the mass spectrum. Figures 2a and 2b show negative and positive ion TDCIMS spectra obtained from 10 nm particles collected for 3 hours.

To our knowledge, these spectra are the first reported of the composition of sub-20 nm diameter laboratory-generated SOA. The positive and negative ion mass spectra are characterized by peak series of homologous compounds, which decrease in intensity at larger m/z due in part to decreased concentration, but also due to ion decomposition during thermal desorption and ionization as well as a decreased transmission efficiency of larger ions through the quadrupole mass spectrometer. We define the “volatility ratio” as the 6 hour mass-normalized ion abundance (background-subtracted peak area divided by the collected aerosol mass) divided by the respective 3 hour mass-normalized ion abundance. If the volatility ratio is close to unity to within experimental uncertainty, the respective ion can be considered non-volatile and thus its abundance is linearly dependent upon collection time. These ions are color-coded red in Figures 2a and 2b and have been termed “non-volatile.” “Semi-volatile” ions (black) corresponded to volatility ratios of between 0.5 and 1. Ions in blue exhibited ratios of less than 0.5, suggesting that these are the most volatile in the recorded mass spectra and are therefore termed “volatile.” From Figures 2a and 2b it can be seen that the negative ion spectrum contains more non-volatile ions compared to the positive ion spectrum, whereas semi-volatile and volatile ions dominate the positive ion mass spectrum. From this analysis it is clear that collection time has an impact on the measured composition, especially in the positive ion mass spectra. Thus in our analysis we shall only compare non-volatile ions (shown in red), which are collection time-independent, for samples collected at different aerosol sizes and over different collection times.

3.2.2. Aerosol Composition and the Effects of Particle Size

[13] Figure S4 in the auxiliary material shows the ratio of the mass-normalized abundance of non-volatile ions in 10 nm particles to that in 20 and 40 nm particles. If this ratio for a given ion is 1, then that ion is present at equal concentration in both 10 nm and larger sized particles. The plot in Figure S4 shows relatively minor differences in the composition of 10 and 20 nm diameter particles, as the ratio is close to unity for all detected non-volatile ions. In contrast, the mass-normalized abundances for most ions in 10 nm diameter particles are approximately twice that of 40 nm particles (ref: Figure S4, open triangles). From this we can conclude that particles of 10 and 20 nm exhibit similar composition, at least for the non-volatile ions detected by the TDCIMS. However, 10 nm particles consist of roughly twice as much non-volatile material as there is in the larger 40 nm particles.

[14] Next, we investigate the specific compounds that contribute to the differences in the composition of 40 nm diameter particles compared to 10 and 20 nm diameter particles. For this analysis we directly compare the composition of 20 nm diameter particles to that of 40 nm diameter particles, since both 20 and 40 nm particles were sampled for the same collection time and therefore biases in the measured composition due to volatility are minimized. Figures 2c and 2d show negative and positive ion mass spectra from 20 nm particles, in which the peaks are classified according to the mass-normalized ion abundance in 20 nm particles divided by that in 40 nm particles. Here, red indicates ions significantly more abundant in 20 nm particles, which we define as those for which the minimum value of the ion in

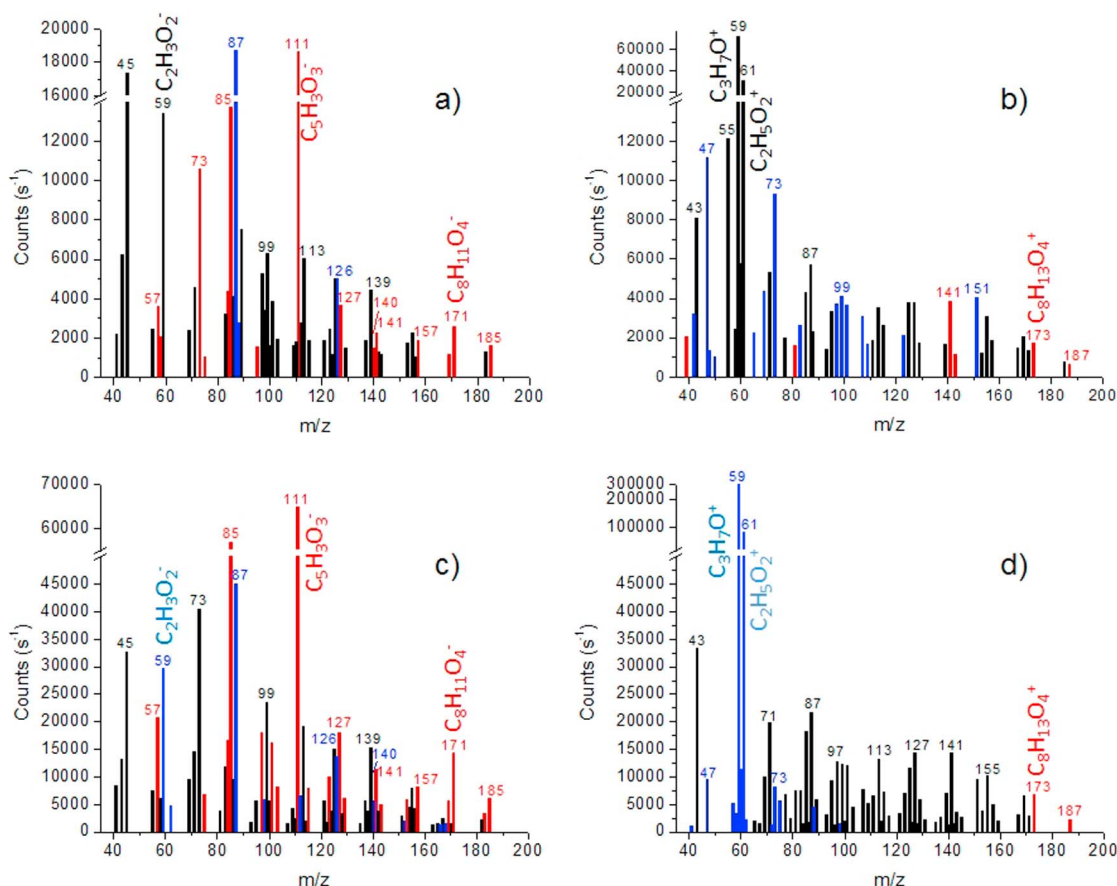


Figure 2. (a) Negative and (b) positive ion spectra from 10 nm particles collected for 3 hours. Mass loadings were determined as 3.1 ng (negative mode) and 2.9 ng (positive). Color-coding refers to different groups of volatility ratios as defined in the text. Red bars indicate “non-volatile” ions with volatility ratios close to one, blue bars refer to ratios of <0.5 and therefore show “volatile” ions. “Semi-volatile” ions are displayed in black and refer to volatility ratios between 0.5 and 1. Formula assignments as determined with the HTOF-TDCIMS are shown for selected ions. Also plotted are (c) negative and (d) positive ion spectra from 20 nm particles collected for 0.5 hours. Mass loadings were determined as 13.9 ng (negative mode) and 12.5 ng (positive). Color-coding refers to the behavior of certain ions when compared to the signal from the 40 nm particles. Red bars indicate ions that dominate in 20 nm particles; blue bars are ions that dominate in 40 nm particles. Black bars represent ions termed equal in both particle sizes.

20 nm particles, after accounting for a 10% uncertainty in the collected mass, does not fall below 150% of the value for 40 nm particles. Plotted in blue are ions that dominate in 40 nm particles, which are defined as those for which the maximum value of the ion in 20 nm particles stays below 90% of the value for 40 nm particles (see also Figure S3). Ions in black did not exceed either of the chosen thresholds and are thus considered equal in both particle sizes. Different thresholds were chosen to better visualize the size dependent particle composition but do not affect the interpretation of these results.

[15] Figures 2c and 2d clearly show different particle composition at different sizes. The negative spectrum is dominated by ions more prevalent in 20 nm diameter particles whereas the overwhelmingly highest ion counts in the positive spectrum indicate their prevalence in 40 nm diameter particles. Interestingly enough, the only two ions in the positive spectrum that appear red (higher concentration in 20 nm diameter particles) are the protonated counterparts of the negative, deprotonated m/z –171 (cis-norpinic and/or terpenylic acid) and –185 (pinic acid) ions [Claeys *et al.*,

2009; Gao *et al.*, 2010]. Both are dicarboxylic acids and well-known constituents of α -pinene initiated SOA and are found in even greater abundance in the negative ion spectrum. While the importance of these species in the growth of nanometer-sized particles has previously been hypothesized from measurements of larger diameter particles [Claeys *et al.*, 2009], we provide evidence of their importance in smallest biogenic nanoparticles from *direct* measurements.

[16] When comparing the color-coded classifications in Figures 2a, 2b, 2c and 2d we observe that all ions with lowest volatility dominate the 10 and 20 nm particle composition, whereas more volatile ions coincide with the appearance of 40 nm particles. Furthermore it is remarkable that, with the exception of one minor ion at m/z –140, none of the ions dominating 20 nm particle composition (red, Figures 2c and 2d) fall in the category “volatile” (blue, Figures 2a and 2b) and vice versa. These observations are therefore consistent with one another and clearly suggest that vapor partitioning to the particle phase is size dependent. This finding is in accordance with the Kelvin equation, which states that higher vapor pressure compounds can partition into larger sized

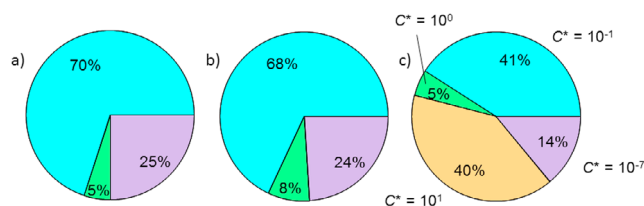


Figure 3. Modeled molar-scale composition as a function of particle size for a parameterized α -pinene + ozone system consisting of four lumped oxidation products and one high molecular weight/low volatility product (see supplement material for model description). Size-dependent composition is shown for (a) 10, (b) 20, and (c) 40 nm particles. Saturation concentrations (C^*) of the compounds are labeled in Figure 3c.

particles, whereas smaller particles require that the condensing species have a lower vapor pressure.

3.2.3. High Resolution Particle Composition Analysis

[17] All results on particle phase composition presented above were obtained using unit mass resolution data from a quadrupole mass spectrometer-based TDCIMS. In separate experiments we applied a High Resolution Time-of-Flight (HTOF)-based TDCIMS to the study of 20 nm particle composition in order to determine exact molecular formulae. Tables S1a, b present results for selected ions representative of the two categories “non-volatile” and “volatile.” Among the most important ions in the negative mode, m/z -171 and -185 were positively identified as $C_8H_{11}O_4^-$ and $C_9H_{13}O_4^-$, respectively. Both formulae agree with the compounds suggested by *Claeys et al.* [2009] and *Gao et al.* [2010].

[18] In the positive ion spectra, m/z $+59$ was assigned to $C_3H_7O^+$, a protonated C_3 carbonyl (acetone), which likely originates from fragmentation of larger molecular weight carbonyl-containing compounds during thermal desorption, chemical ionization, or ion-neutral collisions. In summary, the general picture suggests that the negative mass spectra are dominated by mono- and dicarboxylic acids, whereas the identified ions in the positive spectra include carbonyl-containing compounds as well as protonated organic acids. These molecular assignments are consistent with the species that are expected to react with TDCIMS reagent ions, i.e., $(H_2O)_nH_3O^+$ and $(H_2O)_nO_2^+$ ($n = 0-2$) in positive and negative ion modes, respectively.

4. Comparison to Growth Model

[19] The observed size dependent composition change is also supported by process level modeling of condensational growth. More specifically, the model supports the experimental results that composition is similar between 10 and 20 nm particles, and dissimilar between 10–20 and 40 nm particles. A description of the model is given in the auxiliary material. Figure 3 shows the molar-scale contribution of each model compound to predicted particle growth as a function of particle size for a 10, 20, and 40 nm particle (see Table S2 for description of model compounds; the saturation concentration (C^*) for these compounds are shown in Figure 3c). The single particle growth model reproduces the experimentally-observed changing particle composition as a function of particle size, with carboxylic

acids (or compounds with vapor pressures on the order of 10^{-11} atm or less, corresponding to C^* values of $10^{-1} \mu\text{g m}^{-3}$ or less) contributing to the growth of particles down to 4 nm and multifunctional hydroxy-carbonyls (or compounds with vapor pressures on the order of 10^{-9} atm, or a C^* of $10^1 \mu\text{g m}^{-3}$) contributing to particles >30 nm. Higher-volatility oxidation products are typically formed in greater yields than lower-volatility products, thus once such compounds can contribute to growth as predicted by the Kelvin effect, they will become the dominant species contributing to and accelerating growth. The predicted growth rates for a reacted α -pinene concentration of 10 ppb were 32 nm min^{-1} for a 5 nm particle, 39 nm min^{-1} for a 10 nm particle, and 58 nm min^{-1} for a 40 nm particle. This increase in the predicted growth rates between the 10 and 40 nm particles is due to the contribution of oxidation product “3” to growth (see Table S2). Notably, the calculated growth rates are in good agreement with the experimentally observed rate of $\sim 30 \text{ nm min}^{-1}$. Product 3 has a Kelvin-corrected vapor pressure of 3×10^{-9} atm over a 40 nm particle; that vapor pressure increases to 7×10^{-9} atm over a 10 nm particle. The relatively volatile α -pinene oxidation products, as represented by Products 3 and 4, are unable to overcome the Kelvin effect at particle sizes <30 nm and thus do not contribute to particle growth. However, due to their relatively high abundance, once such compounds do overcome the Kelvin effect (e.g., at 30 nm for Product 3), as demonstrated here, measured and predicted growth rates and composition change significantly. Thus the consistent picture that emerges when comparing both experimental and modeling results is that the Kelvin effect plays a substantial role in determining particle growth rates and composition.

5. Conclusions

[20] Size-selected biogenic nanoparticles formed from the ozonolysis of α -pinene were directly analyzed for their chemical composition using the TDCIMS. While particles with mobility diameters of 10 and 20 nm appear to have similar composition, a composition change is clearly observed for particles with diameters of 40 nm. The smaller particles were enriched in mono- and dicarboxylic acids, while larger particles showed higher concentrations of carbonyl-containing compounds and low molecular weight organic acids. The particle composition change between 20 and 40 nm particles is thus indicative of a growth process governed by the condensation of compounds of steadily increasing vapor pressures. This finding is confirmed by the growth model suggesting a vapor pressure increase of the respective compounds from $\leq 10^{-11}$ atm to $\sim 10^{-9}$ atm. Accordingly, the growth of biogenic nanoparticles is highly sensitive to the Kelvin effect confirming the early work done by *Heisler and Friedlander* [1977].

[21] A comparison of selected compounds detected in the gas phase (Figure 1) to the aerosol phase provides insights into the mechanisms of aerosol growth due to organic compounds. The ions m/z $+173$ and $+187$ are observed in the gas phase using the PTR-TOF-MS, and in addition these gas phase species increase with reaction time. Significantly, ions at the same m/z , as well as the deprotonated counterparts to these ions, are observed in TDCIMS spectra as mentioned previously. One possible interpretation for this observation is

that these species form in the gas phase and directly condense onto newly formed particles.

[22] For the conditions used in the current study the growth due to this mechanism is *very* fast, with growth rates in the order of thousands of nanometers per hour ($\sim 30 \text{ nm min}^{-1}$). This rapid growth may be the reason why we don't see substantial amounts of particles below 10 nm. Whether this is of immediate atmospheric relevance remains to be shown as the concentrations in the flow tube were 1–2 orders of magnitude above ambient levels. However, for a better understanding of nanoparticle growth processes, future research should focus on highly time-resolved particle size measurements.

[23] **Acknowledgments.** This work was supported by the Austrian Science Fund (FWF): J3198-N21 and by US DOE grant DE-SC0006861. J.N.S. acknowledges funding from the Finnish Academy grant 251007 and US NSF grant 0919317. The National Center for Atmospheric Research is supported by NSF.

[24] The Editor thanks two anonymous reviewers for assistance evaluating this paper.

References

- Boy, M., et al. (2005), Sulphuric acid closure and contribution to nucleation mode particle growth, *Atmos. Chem. Phys.*, **5**, 863–878, doi:10.5194/acp-5-863-2005.
- Claeys, M., et al. (2009), Terpenylic acid and related compounds from the oxidation of α pinene: Implications for new particle formation and growth above forests, *Environ. Sci. Technol.*, **43**, 6976–6982, doi:10.1021/es9007596.
- Gao, Y., W. A. Hall, and M. V. Johnston (2010), Molecular composition of monoterpene secondary organic aerosol at low mass loading, *Environ. Sci. Technol.*, **44**, 7897–7902, doi:10.1021/es101861k.
- Hall, W. A., III, and M. V. Johnston (2012), The thermal stability of oligomers in alpha-pinene secondary organic aerosol, *Aerosol Sci. Technol.*, **46**, 983–989, doi:10.1080/02786826.2012.685114.
- Heisler, S. L., and S. K. Friedlander (1977), Gas-to-particle conversion in photochemical smog: Aerosol growth laws and mechanisms for organics, *Atmos. Environ.*, **11**, 157–168, doi:10.1016/0004-6981(77)90220-7.
- Jenkin, M. E. (2004), Modeling the formation and composition of secondary organic aerosol from α - and β -pinene ozonolysis using MCM v3, *Atmos. Chem. Phys.*, **4**, 1741–1757, doi:10.5194/acp-4-1741-2004.
- Jordan, A., et al. (2009), A high resolution and high sensitivity proton-transfer-reaction time-of flight mass spectrometer (PTR-TOF-MS), *Int. J. Mass Spectrom.*, **286**, 122–128, doi:10.1016/j.ijms.2009.07.005.
- Kerminen, V.-M., and M. Kulmala (2002), Analytical formulae connecting the “real” and the “apparent” nucleation rate and the nuclei number concentration for atmospheric nucleation events, *J. Aerosol Sci.*, **33**(4), 609–622, doi:10.1016/S0021-8502(01)00194-X.
- Kirkby, J., et al. (2011), Role of sulfuric acid, ammonia, and galactic cosmic rays in atmospheric aerosol nucleation, *Nature*, **476**, 429–433, doi:10.1038/nature10343.
- Kulmala, M. (2003), How particles nucleate and grow, *Science*, **302**, 1000–1001, doi:10.1126/science.1090848.
- Kulmala, M., et al. (2004), Formation and growth rates of ultrafine atmospheric particles: A review of observations, *J. Aerosol Sci.*, **35**, 143–176, doi:10.1016/j.jaerosci.2003.10.003.
- McMurry, P. H. (1983), New particle formation in the presence of an aerosol: Rates, time scales and sub-0.01 μm size distributions, *J. Colloid Interface Sci.*, **95**(1), 72–80, doi:10.1016/0021-9797(83)90073-5.
- McMurry, P. H., and S. K. Friedlander (1979), New particle formation in the presence of an aerosol, *Atmos. Environ.*, **13**, 1635–1651, doi:10.1016/0004-6981(79)90322-6.
- McMurry, P. H., et al. (2009), Sampling nanoparticles for chemical analysis by low resolution electrical mobility classification, *Environ. Sci. Technol.*, **43**, 4653–4658, doi:10.1021/es8029335.
- Saunders, S. M., et al. (2003), Protocol for the development of the Master Chemical Mechanism, MCM v3 (Part A): Tropospheric degradation of non-aromatic volatile organic compounds, *Atmos. Chem. Phys.*, **3**, 161–180, doi:10.5194/acp-3-161-2003.
- Smith, J. N., et al. (2004), Atmospheric measurements of sub-20 nm diameter particle chemical composition by thermal desorption chemical ionization mass spectrometry, *Aerosol Sci. Technol.*, **38**, 100–110, doi:10.1080/02786820490249036.
- Smith, J. N., M. J. Dunn, T. M. VanReken, K. Iida, M. R. Stolzenburg, P. H. McMurry, and L. G. Huey (2008), Chemical composition of atmospheric nanoparticles formed from nucleation in Tecamac, Mexico: Evidence for an important role for organic species in nanoparticle growth, *Geophys. Res. Lett.*, **35**, L04808, doi:10.1029/2007GL032523.
- Stolzenburg, M. R., P. H. McMurry, H. Sakurai, J. N. Smith, R. L. Mauldin III, F. L. Eisele, and C. F. Clement (2005), Growth rates of freshly nucleated atmospheric particles in Atlanta, *J. Geophys. Res.*, **110**, D22S05, doi:10.1029/2005JD005935.
- Voisin, D., et al. (2003), Thermal desorption chemical ionization mass spectrometer for ultrafine particle chemical composition, *Aerosol Sci. Technol.*, **37**, 471–475, doi:10.1080/02786820300959.
- Weber, R. J., et al. (1997), Measurements of new particle formation and ultrafine particle growth rates at a clean continental site, *J. Geophys. Res.*, **102**(D4), 4375–4385, doi:10.1029/96JD03656.
- Wehner, B., T. Petäjä, M. Boy, C. Engler, W. Birmili, T. Tuch, A. Wiedensohler, and M. Kulmala (2005), The contribution of sulfuric acid and non-volatile compounds on the growth of freshly formed atmospheric aerosols, *Geophys. Res. Lett.*, **32**, L17810, doi:10.1029/2005GL023827.